Development 140, 76-81 (2013) doi:10.1242/dev.080473

Distinct requirements for *wnt9a* and *irf6* in extension and integration mechanisms during zebrafish palate morphogenesis

Max Dougherty[1,2,*], George Kamel[1,2,*], Michael Grimaldi[1,2], Lisa Gfrerer[1,2], Valeriy Shubinets[1,2], Renee Ethier[1,2], Graham Hickey[1,2], Robert A. Cornell[3] and Eric C. Liao[1,2,4,‡]

SUMMARY

Development of the palate in vertebrates involves cranial neural crest migration, convergence of facial prominences and extension of the cartilaginous framework. Dysregulation of palatogenesis results in orofacial clefts, which represent the most common structural birth defects. Detailed analysis of zebrafish palatogenesis revealed distinct mechanisms of palatal morphogenesis: extension, proliferation and integration. We show that *wnt9a* is required for palatal extension, wherein the chondrocytes form a proliferative front, undergo morphological change and intercalate to form the ethmoid plate. Meanwhile, *irf6* is required specifically for integration of facial prominences along a V-shaped seam. This work presents a mechanistic analysis of palate morphogenesis in a clinically relevant context.

KEY WORDS: Palate, *irf6*, *wnt9a*, Cranial neural crest, Craniofacial, Zebrafish

INTRODUCTION

Palate development provides an excellent example of conservation of genetic programs and morphogenesis events across vertebrate ontogeny. Five distinct facial prominences converge to shape the facial form. The median frontonasal prominence (FNP) contributes the columella and the central region of the primary palate, and coalesces with the paired maxillary prominences in a Y-shaped seam, where *Bmp* and a *Pbx*-dependent *Wnt-p63-Irf6* regulatory module acts (Tamarin and Boyde, 1977; Jiang et al., 2006; Depew and Compagnucci, 2008; Ferretti et al., 2011). The secondary palate forms from midline fusion of bilateral palatal shelves, which are derived from the maxillary prominences (MXP), where midline fusion is characterized by distinct palatal shelf movements, apoptosis and epithelial-mesenchymal transition (Cuervo and Covarrubias, 2004; Helms et al., 2005; Bush and Jiang, 2012). Dysregulation of the highly choreographed molecular and morphogenetic events results in orofacial clefts in humans, which represent the most common structural birth defects (Mulliken, 2004; Rahimov et al., 2011).

Wnt signaling is crucial to craniofacial morphogenesis, where a delicate balance of co-receptor LRP6 and the transcriptional co-activator β-catenin mediate head formation at large, and refines specific facial features such as the lip (Brugmann et al., 2007; Fossat et al., 2011). In the mouse, *Wnt9b* is involved in fusion of the medial and lateral nasal processes (Juriloff et al., 2006; Lan et al., 2006; Ferretti et al., 2011). Variation of Wnt genes is associated with non-syndromic cleft lip and/or palate (CLP) in human and mouse studies (Juriloff et al., 2006; Chiquet et al., 2008). Knockdown of zebrafish *wnt9a* results in an abridged palate, where the bilateral trabeculae are joined in the midline but the ethmoid plate does not extend (Curtin et al., 2010). Conservation of genetic regulation and analogy of facial prominences between amniotes and zebrafish has been carefully described (Swartz et al., 2011).

The *IRF6* transcription factor is a key regulator of palatogenesis, implicated in both syndromic and non-syndromic CLP (Kondo et al., 2002; Beaty et al., 2010). Irf6 regulates the transition of keratinocyte between proliferation and differentiation, and the craniofacial abnormalities observed in the *Irf6* mouse mutants may be secondary to the abnormal differentiation of epithelial tissues, including epidermis and oral epithelium (Ingraham et al., 2006; Richardson et al., 2006; Richardson et al., 2009). Expression of *irf6* in zebrafish has been reported in the pharyngeal arches and oral epithelium, and its embryonic requirement has been examined using dominant-negative mRNA overexpression that resulted in epiboly arrest, precluding analysis of its potential role in palatogenesis (Ben et al., 2005; Sabel et al., 2009). The function of *Irf6* has been described for epithelial development in murine and zebrafish models, but whether and how this gene may directly regulate palatal fusion remains unclear (Sabel et al., 2009; Restivo et al., 2011; de la Garza et al., 2012).

This work presents detailed analysis of zebrafish palatogenesis, demonstrating that *wnt9a* and *irf6* are required for distinct morphogenetic processes. *wnt9a* is required for coordinated extension, cell proliferation, morphological change and intercalation of the palatal chondrocytes. Meanwhile, *irf6* is expressed in the bilateral MXP chondrocytes and required for integration with the median FNP. The morphogenetic context in which to understand a clinically relevant zebrafish orofacial cleft model is proposed, which could be applied towards future studies of palatogenesis in this highly tractable vertebrate system.

MATERIALS AND METHODS

Zebrafish lines and maintenance

Zebrafish husbandry was performed as described previously (Westerfield, 1993). The *Tg(sox10:kaede)* line was generated using the 7.2 kb genomic

[1]Center for Regenerative Medicine, Massachusetts General Hospital, Harvard Medical School, Boston, MA 02114, USA. [2]Division of Plastic and Reconstructive Surgery, Massachusetts General Hospital, Harvard Medical School, Boston, MA 02114, USA. [3]Department of Anatomy and Cell Biology, Carver College of Medicine, University of Iowa, Iowa City, IA 52242, USA. [4]Harvard Stem Cell Institute, Boston, MA 02114, USA.

*These authors contributed equally to this work
‡Author for correspondence (cliao@partners.org)

Accepted 16 October 2012

region upstream of zebrafish *sox10* (a gift from R. Kelsh, University of Bath, UK) and the kaede protein sequence using Gateway cloning (Invitrogen) (Kwan et al., 2007; Dutton et al., 2008).

Generation of *irf6* dominant-negative mutants

Site-directed mutagenesis of *irf6* was performed using the QuikChange II XL Kit (Agilent Technologies), which substitutes the critical arginine 84 residue: R84C, R84H and R84K. Each mutant transgenic, *Tg(sox10:irf6^{R84C,H,K})*, was generated with *irf6* driven by the *sox10* promoter, with germline integration mediate by Tol2 transposase.

RNA *in situ* hybridization and immunohistochemistry

Whole-mount RNA *in situ* hybridization was performed as described previously (Thisse and Thisse, 2008), with DIG- and DNP-labeled *irf6* probe using Cyanine5 on *sox10:GFP* embryos, followed by incubation with anti-GFP Alexa Fluor 488 conjugate (Invitrogen).

Antisera against human IRF6 (anti-IRF6 peptide, 358-HQKGQIEKQPPFEIY-372 Genway Biotech) and against zebrafish Irf6 (i.e. anti-Irf6 peptides 137-TYETDGDEDDIPDTPE-152 and 213-ANVWPKKEPEDVEM-226, affinity purified; B. Schutte and R.C., unpublished) were used as previously reported (Fakhouri et al., 2012).

Proliferation and apoptosis assays

Proliferation was detected using the Click-iT EdU Alexa Fluor 488 Imaging Kit (Invitrogen). Apoptosis was detected using the Click-iT TUNEL Alexa Fluor 488 Imaging Assay. Detection was performed in the background of *sox10:mcherry* in analysis of *wnt9a* morphants. The *Tg(sox10:irf6^{R84C,H,K})* and *Tg(sox10:kaede)* lines were crossed to label neural crest cells in the *irf6* mutants.

Lineage analysis and imaging

Photoconversion was performed using the UV laser (404.3 nm) for 5-30 seconds, performed unilaterally so that the contralateral side serves as internal control. For time-lapse imaging, embryos were mounted in low-melt agarose, continuously imaged (2-4 minute intervals) over 24-36 hours.

RESULTS AND DISCUSSION

Zebrafish palate morphogenesis

Lineage tracing of migrating cranial neural crest cells (CNCCs) was carried out using the *sox10:kaede* transgenic (Dougherty et al., 2012). We confirmed that at 16 hours post-fertilization (hpf), the median and lateral ethmoid plate could be targeted by photoconversion of the CNCCs anterior and medial to the developing eye, respectively (Fig. 1A,B) (Wada et al., 2005; Eberhart et al., 2006). More specific CNCC labeling could be achieved by photoconverting at 19 hpf, where a small group of cells has already extended ventrally at the most anterior boundary of the embryo; these are the cells that will stream to form the median ethmoid plate (Fig. 1C,F,G; supplementary material Movies 1-3). This anterior group of CNCCs has been suggested to be analogous to the frontonasal process (FNP) (Swartz et al., 2011).

Time-lapse confocal analysis revealed that migration of the anterior-most CNCCs to the median ethmoid plate can be divided into three stages. First, CNCCs in discrete paired lateral anterior populations merge at the midline, while transitioning from a rostral to caudal direction of migration (supplementary material Movie 1). Second, the cells converge towards the midline as they extend into the space over the oral cavity and in between the developing paired maxillary process (MXP) positioned laterally (supplementary material Movie 2). Third, the frontonasal CNCCs make a sharp 180° turn at the anterior boundary of the embryo, while condensing to form a single median stream that then migrates caudally to meet the paired MXP that extend cephalad (supplementary material Movie 3).

When the entire length of the extending MXP was photoconverted, one can observe that the palate extension occurs via two distinct mechanisms: morphological change and proliferation. Extension of the lateral palate element results from morphological change of the chondrocytes into a columnar shape and intercalation in a cobblestone stacked pattern, leading to a gain in the length of the photoconverted area (bracket, Fig. 1E). Meanwhile, additional unlabeled green cells are observed to proliferate beyond the photoconverted red region, extending anteriorly to form the distal part of the ethmoid plate (asterisk bracket, Fig. 1E; supplementary material Movie 4). In fact, supplementary material Movie 4 shows both accumulation of cells in the proliferative front (anterior of the red photoconverted region) and stacking of columnar cells proximally. Palatal extension occurs by a similar mechanism to that previously described for the lower jaw, where mandible extension is mediated in part by morphological change and arrangement of chondrocytes into an intercalated pattern (Kimmel et al., 1998; Kimmel et al., 2001).

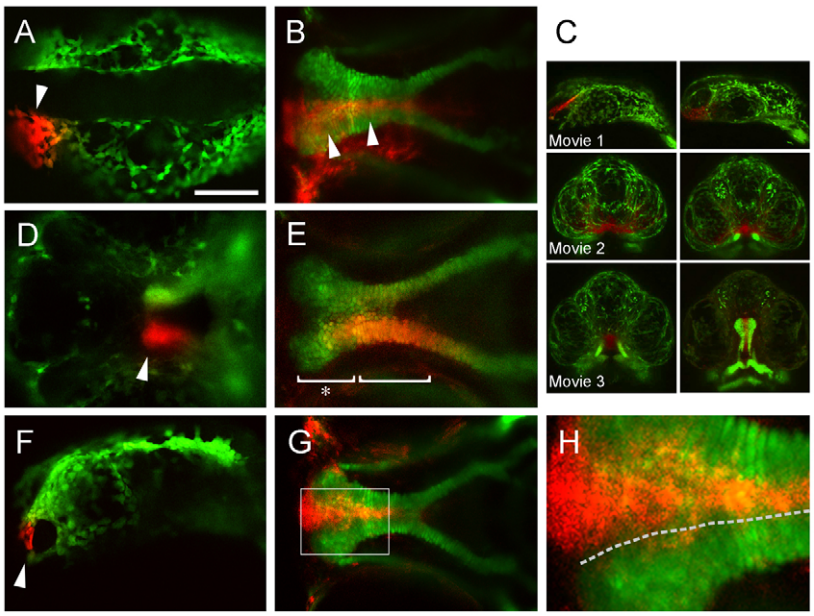

Fig. 1. Palate morphogenesis in zebrafish. (**A**,**B**) The anterior cells at 14-somites (arrowhead, A) tracked to the median ethmoid plate at 4.5 dpf (arrowheads, B). (**C**) Screenshots of time-lapse movies capturing this process. (**D**,**E**) Unilateral labeling of the entire maxillary prominence at 55 hpf (arrowhead, D) revealed that the mature lateral ethmoid plate and trabeculae are formed both by uniform expansion (bracket, E) as well as increased proliferation at the leading edge (asterisk) (see also Fig. 2C, supplementary material Movie 4). (**F**,**G**) Photoconversion of FNP cells at 20 somites (F arrowhead) labeled only the median ethmoid at 4.5 dpf (G), also captured in supplementary material Movies 1-3. (**H**) Enlargement of inset in G. Inspection of the ethmoid plate revealed that labeled CNCCs could be traced along the seam (broken line) between the median and lateral ethmoid plate; lateral to this line, chondrocytes are columnar in appearance while medially they are cuboidal. A, dorsal view; F, lateral view; B,D,E,G,H, ventral views. Scale bar: 50 μm.

As the median ethmoid plate merges with the paired lateral MXP, a morphologically discrete transition can be delineated, which represents a morphologically defined border between juxtaposed columnar-shaped cells of the lateral ethmoid plate element and the cuboidal-shaped cells of the median ethmoid plate (broken line, Fig. 1H). Along this morphological transition, the red/green fluorescence appears to respect the delineation of median versus lateral ethmoid plate.

The amniote upper lip and primary palate forms from fusion of the MXP with the FNP derivatives of medial and lateral nasal processes. In the zebrafish, the ethmoid plate is also formed from convergence of three parts: the paired MXP (trabeculae) extending from lateral to medial and the FNP (median ethmoid plate) that streams along the midline in a rostral to caudal direction (supplementary material Movies 2, 3). We propose the V-shaped fusion seam between the median FNP and the bilateral MXP of the zebrafish palate is analogous to the Y-shaped junction found in the palate of amniotes, supported from molecular and morphogenetic evidence presented here and previously (Ferretti et al., 2011; Swartz et al., 2011). In this light, zebrafish palatogenesis is analogous to formation of the amniote lip/primary palate unit. With this model of zebrafish palatogenesis in mind, we explored whether mechanisms resulting in cleft malformation are also conserved.

wnt9a is required for palatal extension

In mouse models, cleft lip and palate can form as a result of defects in cell proliferation where the palatal shelves fail to extend, thereby precluding midline union, exemplified by targeted disruption of *Tgfbr2* (Ito et al., 2003). The analogous defect in zebrafish palatogenesis would be failure in extension mechanisms of the MXP, which one may predict will result in a short ethmoid plate. In fact, when genes required for murine palatogenesis are targeted via morpholino knockdown in zebrafish, such as *fgf10*, *tgfb2* and *pax9*, shortened ethmoid plate phenotypes were observed (Swartz et al., 2011). Similarly, when zebrafish *wnt9a* (ortholog of human *WNT9B*) was disrupted by morpholino knockdown, a short ethmoid plate phenotype was reported (Curtin et al., 2010). Knockdown of *wnt9a* in *col2a:GFP* transgenic embryos confirmed that the short ethmoid plate phenotype is a result of absent chondrocytes, not a consequence of immature chondrocytes that failed to deposit glycosaminoglycans and therefore were undetected by Alcian Blue staining (Fig. 2A,B). Likewise, Wnt regulation of the convergence extension process during zebrafish embryogenesis has been described, where disruption of Wnt/planar cell polarity in the zebrafish *gpc4* mutant also resulted in foreshortened ethmoid plate (Verkade and Heath, 2008; LeClair et al., 2009).

Extension of the palate requires morphological change of the chondrocytes and cell proliferation, both of which were disrupted in the *wnt9a* morphant. In the *wnt9a* morphant, chondrocytes failed to adopt a columnar shape and do not stack in an intercalated pattern (Fig. 2). Lineage analysis of the *wnt9a* morphant confirmed that the short ethmoid plate phenotype did not result from failed migration of the frontonasal CNCC population, which in fact still migrated to the median ethmoid plate (supplementary material Fig. S1). However, proliferation of cells in the ethmoid plate was decreased in the *wnt9a* morphant (Fig. 2C, arrow). Lack of extension is not due to increased cell death, confirmed by TUNEL assay in the morphant (Fig. 2E,F). The proliferation defect can also be demonstrated by time-lapse confocal imaging in the *Tg(sox10:kaede)* embryo, where new green chondrocytes accrued distal to the red photoconverted region in the wild type

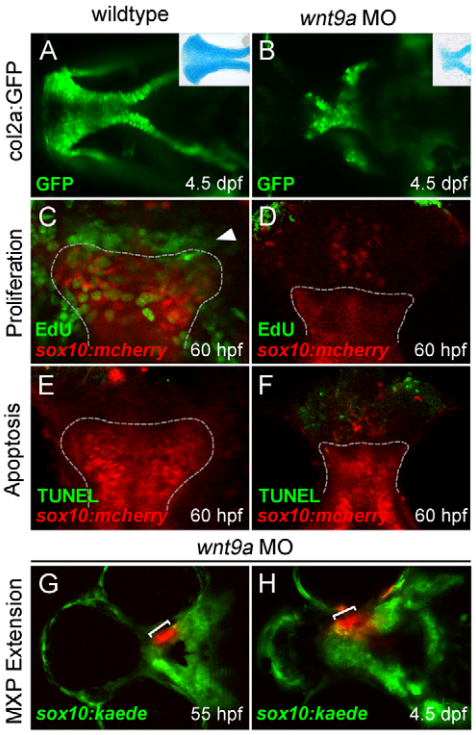

Fig. 2. *wnt9a* knockdown results in failure of maxillary extension. (**A**,**B**) *wnt9a* knockdown in the *col2a:GFP* transgenic (B) produced an ethmoid plate similar to that seen by Alcian Blue stain (inset, B). (**C**,**D**) EdU staining from 55-60 hpf revealed a proliferative front in the leading edge of the extending ethmoid plate during palatogenesis (arrowhead, C), but absence of new cell divisions in morphants (D). (**E**,**F**) TUNEL assay shows the shortened ethmoid plate (outlined) is not a result of increased cell death. (**G**,**H**) When maxillary process CNCCs were labeled by kaede photoconversion before maxillary extension (bracket, G), they failed to extend significantly by 4.5 dpf (H). All images are ventral views, anterior leftwards.

(supplementary material Movie 4), but were absent in the *wnt9a* morphant (supplementary material Movie 5), as the photoconverted region failed to lengthen (Fig. 2G,H). Together, these results show that *wnt9a* is required for ethmoid plate extension, regulating mechanisms of morphological change and cell proliferation.

irf6 is required for palatal integration

Human recessive or dominant-negative mutations in *IRF6* result in cleft lip and palate, confirmed by similar mutations in the mouse (Kondo et al., 2002; Ingraham et al., 2006; Richardson et al., 2006). An analogous cleft defect in zebrafish may be predicted to manifest as a cleft in the seam where the facial prominences converge, as median ethmoid plate (FNP) and the lateral ethmoid plate (MXP) converge and integrate along an analogous V-shaped junction.

Embryos injected with dominant-negative truncation mutant *irf6* mRNA resulted in epiboly arrest, precluding analysis of *irf6* function in palatogenesis (Sabel et al., 2009; de la Garza et al., 2012). It has been reported that *irf6* is expressed in pharyngeal arch epithelium and that *sox10* is expressed in pharyngeal arch mesenchyme (Ben et al., 2005; Dutton et al., 2008; Sabel et al., 2009). We confirmed that *irf6* is expressed in the pharyngeal arch epithelium at 55 hpf but also detected an overlap between *irf6* and *GFP* in the pharyngeal arch mesenchyme of *Tg(sox10:gfp)* transgenic embryos at this stage (Fig. 3A-C). Moreover, at 72 hpf,

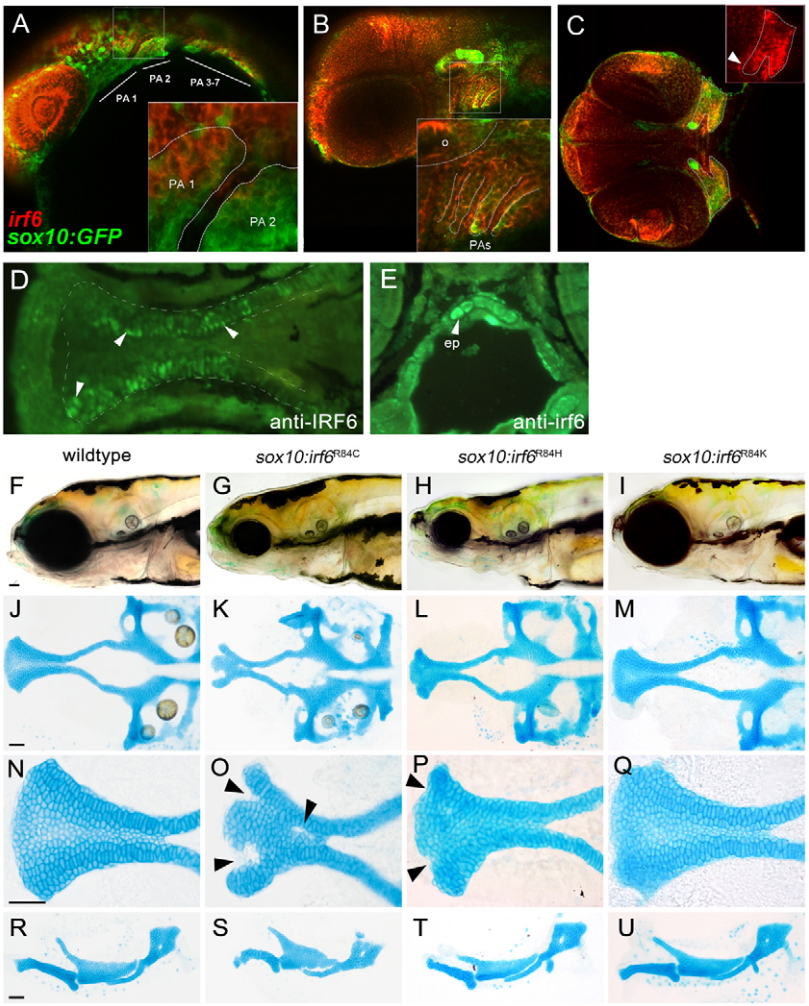

Fig. 3. Expression analysis of endogenous *irf6* and functional analysis of *sox10:irf6*^{R84C,H,K} mutants. (A-E) RNA *in situ* hybridization demonstrated extensive overlap of endogenous *irf6* expression with *sox10*-labeled CNCCs. (**A**) At 24 hpf, *irf6* expression can be found pharyngeal arches. (**B**) By 48 hpf, *irf6* expression is detected in both the pharyngeal mesenchyme and pharyngeal ectoderm. (**C**) By 55 hpf, *irf6* expression is detected in the converging maxillary and mandibular prominences (inset). (**D**,**E**) Immunohistochemistry at 72 hpf using antisera against non-overlapping epitope of human IRF6 (D) and zebrafish irf6 (E), each with specific staining in the ethmoid plate, shown in ventral and cross-sectional views. Arrowheads indicate ethmoid plate chondrocytes. (**F-Q**) Comparison of wild-type and mutant craniofacial structures, with live images (F-I), dissected neurocranium (J-M), flat-mounted lower jaw structures (**R-U**) at 10× magnification and ethmoid plate (N-Q) at 40× magnification. The R84C cleft phenotype is the most severe (arrowheads, O). R84H has a milder cleft phenotype, with subtle indentations at the anterior edge of the seam between median and lateral ethmoid (arrowheads, P), whereas the conserved amino acid substitution R84K appears wild type. ep, ethmoid plate; PA, pharyngeal arch; o, otic vesicle.

anti-irf6 immunoreactivity was clearly demonstrated in ethmoid plate chondrocytes (Fig. 3D,E). Therefore, to circumvent the gastrulation lethality of dominant-negative *irf6* mRNA injection, we expressed *irf6* dominant-negative mutant transgenes under transcriptional control of the *sox10* promoter, to ascertain their function during palatogenesis.

Dominant-negative *irf6* mutants were generated based on known human mutations that abrogate DNA binding, where arginine 84 plays a crucial role (Escalante et al., 1998; Kondo et al., 2002; Item et al., 2005). Three mutant *irf6* transgenes were generated: two transgenes harbor disruptive amino acid substitutions (R84C, R84H), and one transgene contained a conserved amino acid change (R84K) to serve as negative control. Stable transgenic lines of each arginine mutant were generated, where *Tg(sox10:irf6*^{R84C,H,K}*)* embryos assayed using *irf6* riboprobe at 10-somites shows *sox10* pattern of expression, a time when endogenous *irf6* is normally absent, thereby confirming high level transgene expression (supplementary material Fig. S2). Expression of *irf6* mutants under transcriptional control of *sox10* did not perturb early neural crest patterning, with wild-type expression of *dlx2a* and *sox9a* (supplementary material Fig. S2).

The *irf6* mutant embryos appeared grossly normal during early embryogenesis; however, the overall head shape of the R84C and R84H mutants become noticeably smaller than wild type past the pharyngeal stages (Fig. 3F-I). When stained with Alcian Blue, R84C and R84H mutants exhibited clefts between the median FNP and paired MXP elements, along the V-shaped seam by which they are joined (Fig. 3J-Q). In particular, clefts in the R84C mutant were more severe than the R84H mutant, whereas R84K appeared wild type, consistent with degree of non-conserved amino acid substitutions. Time-lapse visualization of the ethmoid plate demonstrated that although new chondrocytes appeared in the distal front of the paired MXP as the median FNP chondrocytes emerged, the median FNP and paired MXP failed to integrate and form a continuous ethmoid plate (supplementary material Movie 6).

The lower jaw was also dysmorphic in R84C and R84H mutants with shortened Meckel's cartilage and smaller palatoquadrate structures, again with R84C>R84H in severity of phenotype (Fig. 3R-U). It is important to note that the dominant-negative *irf6* mutants affected integration of the median FNP with the paired MXP specifically, whereas extension of the formed ethmoid plate was not affected; the chondrocytes were able to differentiate and adopt columnar morphology, and organized in the intercalated pattern.

Zebrafish model of palatogenesis

The CNCC lineage analysis presented here illustrates conservation of the fundamental morphogenetic events between amniote primary palate and zebrafish ethmoid plate. Moreover, we describe distinct mechanisms of palatal extension at the cellular level: morphological change, intercalation, proliferation and integration

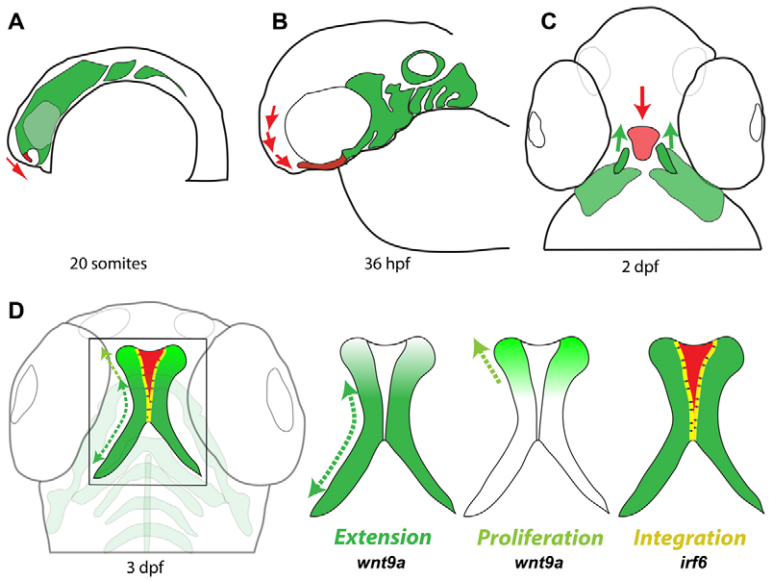

Fig. 4. Summary of zebrafish palatogenesis. (**A**) At 20 somites, the paired groups of the frontonasal CNCC stream change from a rostral to caudal direction of migration, while simultaneously converging to the midline. (**B**) By 36 hpf, these cells migrate under the eye. (**C**) At 2 dpf, the FNP begins to coalesce, while the paired maxillary prominences extend medially and cephalad. (**D**) By 3 dpf, the maxillary prominence forms the lateral ethmoid plate by extension and proliferation. At the same time, a process of integration joins the lateral maxillary elements with the median frontonasal element in a V-shaped junction (yellow dashed line).

(Fig. 4). Distinct requirements of *wnt9a* and *irf6* in palatal extension and integration, respectively, reveal the complex molecular control of palatogenesis. These findings raise the issue of whether orofacial clefts in individuals with Van der Woude syndrome, where *IRF6* is mutated, result from disruption of *IRF6*-mediated events within the palatal chondrocytes or within oral epithelium, or within both.

Acknowledgements
We are grateful to Brian Schutte for generating and sharing the anti-zebrafish-irf6 sera, to Greg Bonde for technical assistance, to Robert Kelsh for kindly sharing the zebrafish *sox10* promoter genomic DNA, and to Renee Ethier for excellent management of our aquatics facility.

Funding
E.C.L. received generous support from the March of Dimes Basil O'Connor Starter Scholar Award, from Shriners Hospital for Children, from the American Surgical Association and from the Plastic Surgery Foundation. G.K. was supported by the Plastic Surgery Foundation. V.S. was supported by Howard Hughes Medical Institute Medical Student Research Award.

Competing interests statement
The authors declare no competing financial interests.

Supplementary material
Supplementary material available online at
http://dev.biologists.org/lookup/suppl/doi:10.1242/dev.080473/-/DC1

References

Beaty, T. H., Murray, J. C., Marazita, M. L., Munger, R. G., Ruczinski, I., Hetmanski, J. B., Liang, K. Y., Wu, T., Murray, T., Fallin, M. D. et al. (2010). A genome-wide association study of cleft lip with and without cleft palate identifies risk variants near MAFB and ABCA4. *Nat. Genet.* **42**, 525-529.
Ben, J., Jabs, E. W. and Chong, S. S. (2005). Genomic, cDNA and embryonic expression analysis of zebrafish IRF6, the gene mutated in the human oral clefting disorders Van der Woude and popliteal pterygium syndromes. *Gene Expr. Patterns* **5**, 629-638.
Brugmann, S. A., Goodnough, L. H., Gregorieff, A., Leucht, P., ten Berge, D., Fuerer, C., Clevers, H., Nusse, R. and Helms, J. A. (2007). Wnt signaling mediates regional specification in the vertebrate face. *Development* **134**, 3283-3295.
Bush, J. O. and Jiang, R. (2012). Palatogenesis: morphogenetic and molecular mechanisms of secondary palate development. *Development* **139**, 231-243.
Chiquet, B. T., Blanton, S. H., Burt, A., Ma, D., Stal, S., Mulliken, J. B. and Hecht, J. T. (2008). Variation in WNT genes is associated with non-syndromic cleft lip with or without cleft palate. *Hum. Mol. Genet.* **17**, 2212-2218.
Cuervo, R. and Covarrubias, L. (2004). Death is the major fate of medial edge epithelial cells and the cause of basal lamina degradation during palatogenesis. *Development* **131**, 15-24.
Curtin, E., Hickey, G., Kamel, G., Davidson, A. J. and Liao, E. C. (2011). Zebrafish wnt9a is expressed in pharyngeal ectoderm and is required for palate and lower jaw development. *Mech. Dev.* **128**, 104-115.
de la Garza, G., Schleiffarth, J. R., Dunnwald, M., Mankad, A., Weirather, J. L., Bonde, G., Butcher, S., Mansour, T. A., Kousa, Y. A., Fukazawa, C. F. et al. (2012) Interferon regulatory factor 6 promotes differentiation of the periderm by activating expression of grainyhead-like 3. *J. Invest. Dermatol.* **2012**, doi:10.1038/jid.2012.269.
Depew, M. J. and Compagnucci, C. (2008). Tweaking the hinge and caps: testing a model of the organization of jaws. *J. Exp. Zool.* **310B**, 315-335.
Dougherty, M., Kamel, G., Shubinets, V., Hickey, G., Grimaldi, M. and Liao, E. C. (2012). Embryonic fate map of first pharyngeal arch structures in the sox10: kaede zebrafish transgenic model. *J. Craniofac. Surg.* **23**, 1333-1337.
Dutton, J. R., Antonellis, A., Carney, T. J., Rodrigues, F. S., Pavan, W. J., Ward, A. and Kelsh, R. N. (2008). An evolutionarily conserved intronic region controls the spatiotemporal expression of the transcription factor Sox10. *BMC Dev. Biol.* **8**, 105.
Eberhart, J. K., Swartz, M. E., Crump, J. G. and Kimmel, C. B. (2006). Early Hedgehog signaling from neural to oral epithelium organizes anterior craniofacial development. *Development* **133**, 1069-1077.
Escalante, C. R., Yie, J., Thanos, D. and Aggarwal, A. K. (1998). Structure of IRF-1 with bound DNA reveals determinants of interferon regulation. *Nature* **391**, 103-106.
Fakhouri, W. D., Rhea, L., Du, T., Sweezer, E., Morrison, H., Fitzpatrick, D., Yang, B., Dunnwald, M. and Schutte, B. C. (2012). MCS9.7 enhancer activity is highly, but not completely, associated with expression of Irf6 and p63. *Dev. Dyn.* **241**, 340-349.
Ferretti, E., Li, B., Zewdu, R., Wells, V., Hebert, J. M., Karner, C., Anderson, M. J., Williams, T., Dixon, J., Dixon, M. J. et al. (2011). A conserved Pbx-Wnt-p63-Irf6 regulatory module controls face morphogenesis by promoting epithelial apoptosis. *Dev. Cell* **21**, 627-641.
Fossat, N., Jones, V., Khoo, P. L., Bogani, D., Hardy, A., Steiner, K., Mukhopadhyay, M., Westphal, H., Nolan, P. M., Arkell, R. et al. (2011). Stringent requirement of a proper level of canonical WNT signalling activity for head formation in mouse embryo. *Development* **138**, 667-676.
Helms, J. A., Cordero, D. and Tapadia, M. D. (2005). New insights into craniofacial morphogenesis. *Development* **132**, 851-861.
Ingraham, C. R., Kinoshita, A., Kondo, S., Yang, B., Sajan, S., Trout, K. J., Malik, M. I., Dunnwald, M., Goudy, S. L., Lovett, M. et al. (2006). Abnormal skin, limb and craniofacial morphogenesis in mice deficient for interferon regulatory factor 6 (Irf6). *Nat. Genet.* **38**, 1335-1340.
Item, C. B., Turhani, D., Thurnher, D., Yerit, K., Sinko, K., Wittwer, G., Adeyemo, W. L., Frei, K., Erginel-Unaltuna, N., Watzinger, F. et al. (2005). Van Der Woude syndrome: variable penetrance of a novel mutation (p.Arg 84Gly) of the IRF6 gene in a Turkish family. *Int. J. Mol. Med.* **15**, 247-251.
Ito, Y., Yeo, J. Y., Chytil, A., Han, J., Bringas, P., Jr, Nakajima, A., Shuler, C. F., Moses, H. L. and Chai, Y. (2003). Conditional inactivation of Tgfbr2 in cranial neural crest causes cleft palate and calvaria defects. *Development* **130**, 5269-5280.
Jiang, R., Bush, J. O. and Lidral, A. C. (2006). Development of the upper lip: morphogenetic and molecular mechanisms. *Dev. Dyn.* **235**, 1152-1166.

Juriloff, D. M., Harris, M. J., McMahon, A. P., Carroll, T. J. and Lidral, A. C. (2006). Wnt9b is the mutated gene involved in multifactorial nonsyndromic cleft lip with or without cleft palate in A/WySn mice, as confirmed by a genetic complementation test. *Birth Defects Res. A Clin. Mol. Teratol.* **76**, 574-579.
Kimmel, C. B., Miller, C. T., Kruze, G., Ullmann, B., BreMiller, R. A., Larison, K. D. and Snyder, H. C. (1998). The shaping of pharyngeal cartilages during early development of the zebrafish. *Dev. Biol.* **203**, 245-263.
Kimmel, C. B., Miller, C. T. and Moens, C. B. (2001). Specification and morphogenesis of the zebrafish larval head skeleton. *Dev. Biol.* **233**, 239-257.
Kondo, S., Schutte, B. C., Richardson, R. J., Bjork, B. C., Knight, A. S., Watanabe, Y., Howard, E., de Lima, R. L., Daack-Hirsch, S., Sander, A. et al. (2002). Mutations in IRF6 cause Van der Woude and popliteal pterygium syndromes. *Nat. Genet.* **32**, 285-289.
Kwan, K. M., Fujimoto, E., Grabher, C., Mangum, B. D., Hardy, M. E., Campbell, D. S., Parant, J. M., Yost, H. J., Kanki, J. P. and Chien, C. B. (2007). The Tol2kit: a multisite gateway-based construction kit for Tol2 transposon transgenesis constructs. *Dev. Dyn.* **236**, 3088-3099.
Lan, Y., Ryan, R. C., Zhang, Z., Bullard, S. A., Bush, J. O., Maltby, K. M., Lidral, A. C. and Jiang, R. (2006). Expression of Wnt9b and activation of canonical Wnt signaling during midfacial morphogenesis in mice. *Dev. Dyn.* **235**, 1448-1454.
LeClair, E. E., Mui, S. R., Huang, A., Topczewska, J. M. and Topczewski, J. (2009). Craniofacial skeletal defects of adult zebrafish Glypican 4 (knypek) mutants. *Dev. Dyn.* **238**, 2550-2563.
Mulliken, J. B. (2004). The changing faces of children with cleft lip and palate. *N. Engl. J. Med.* **351**, 745-747.
Rahimov, F., Jugessur, A. and Murray, J. C. (2012). Genetics of nonsyndromic orofacial clefts. *Cleft Palate Craniofac. J.* **49**, 73-91.
Restivo, G., Nguyen, B. C., Dziunycz, P., Ristorcelli, E., Ryan, R. J., Ozuysal, O. Y., Di Piazza, M., Radtke, F., Dixon, M. J., Hofbauer, G. F. et al. (2011). IRF6 is a mediator of Notch pro-differentiation and tumour suppressive function in keratinocytes. *EMBO J* doi: 10.1038/emboj.2011.325.
Richardson, R. J., Dixon, J., Malhotra, S., Hardman, M. J., Knowles, L., Boot-Handford, R. P., Shore, P., Whitmarsh, A. and Dixon, M. J. (2006). Irf6 is a key determinant of the keratinocyte proliferation-differentiation switch. *Nat. Genet.* **38**, 1329-1334.
Richardson, R. J., Dixon, J., Jiang, R. and Dixon, M. J. (2009). Integration of IRF6 and Jagged2 signalling is essential for controlling palatal adhesion and fusion competence. *Hum. Mol. Genet.* **18**, 2632-2642.
Sabel, J. L., d'Alençon, C., O'Brien, E. K., Van Otterloo, E., Lutz, K., Cuykendall, T. N., Schutte, B. C., Houston, D. W. and Cornell, R. A. (2009). Maternal Interferon Regulatory Factor 6 is required for the differentiation of primary superficial epithelia in Danio and *Xenopus* embryos. *Dev. Biol.* **325**, 249-262.
Swartz, M. E., Sheehan-Rooney, K., Dixon, M. J. and Eberhart, J. K. (2011). Examination of a palatogenic gene program in zebrafish. *Dev. Dyn.* **240**, 2204-2220.
Tamarin, A. and Boyde, A. (1977). Facial and visceral arch development in the mouse embryo: a study by scanning electron microscopy. *J. Anat.* **124**, 563-580.
Thisse, C. and Thisse, B. (2008). High-resolution *in situ* hybridization to whole-mount zebrafish embryos. *Nat. Protoc.* **3**, 59-69.
Verkade, H. and Heath, J. K. (2008). Wnt signaling mediates diverse developmental processes in zebrafish. *Methods Mol. Biol.* **469**, 225-251.
Wada, N., Javidan, Y., Nelson, S., Carney, T. J., Kelsh, R. N. and Schilling, T. F. (2005). Hedgehog signaling is required for cranial neural crest morphogenesis and chondrogenesis at the midline in the zebrafish skull. *Development* **132**, 3977-3988.
Westerfield, M. (1993). *The Zebrafish Book: A Guide for the Laboratory Use of Zebrafish (Brachydanio rerio)*. Eugene, OR: University of Oregon Press.

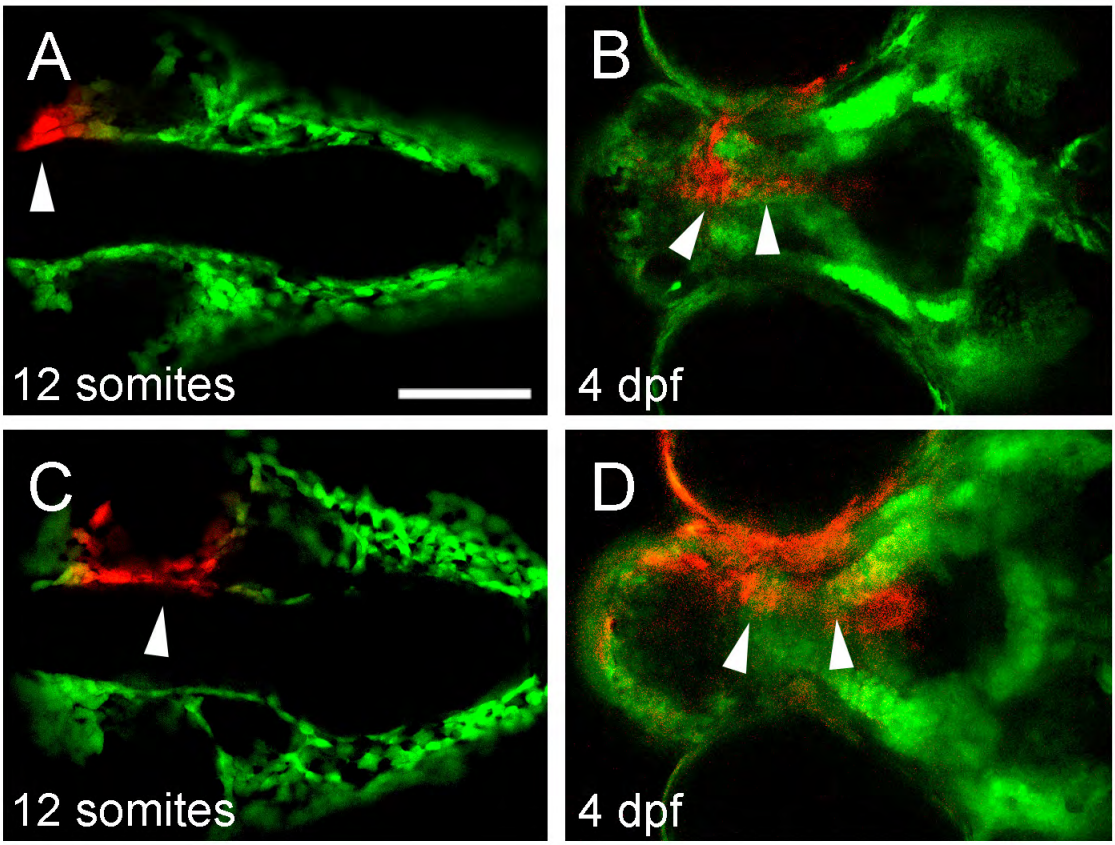

Fig. S1. Lineage analysis of cranial neural crest in *wnt9a* morphant. (**A-D**) CNCCs anterior to the eye, which are destined to form the median ethmoid plate (arrow, A), still migrate to the median region of the dysmorphic and foreshortened ethmoid plate (arrows, B), whereas cells medial to the eye, which are destined to form the lateral ethmoid plate (arrow, C) also reach their destination at 4.5 dpf (arrows, D), indicating that the shortened ethmoid plate is not a result of failure of early CNCC migration. Scale bar: 50 μm.

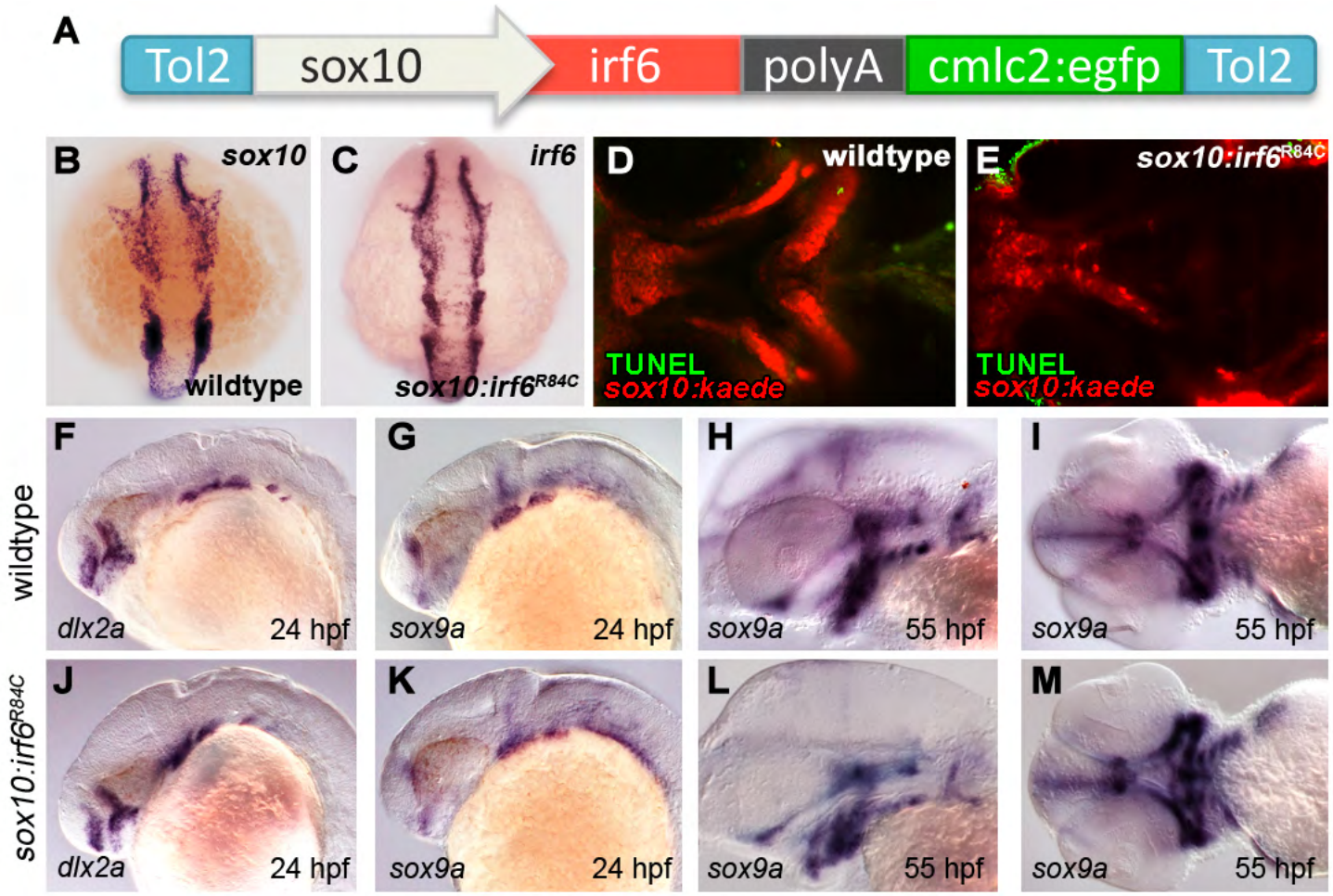

Fig. S2. Characterization of *sox10:irf6*^{R84C} transgenics. (**A**) Transgene contains mutant *irf6* (R84C, R84H, or R84K) under the control of the *sox10* promoter, followed by a fluorescent tag (*cmlc2:egfp*) to facilitate screening. (**B**,**C**) Expression pattern of exogenous *irf6* matches that of *sox10* at 10 somites. (**D**,**E**) TUNEL assay for apoptosis confirms that clefting in *sox10:*^{irf6R84C} is not a result of cell death. (**F**,**G**,**J**,**K**) Expression analysis of neural crest markers *dlx2a* and *sox9a* show that early neural crest development is not significantly affected in the *irf6* mutant. (**F**,**J**) At 24 hpf, the expression pattern of *dlx2a* is unaffected in the developing pharyngeal arches. (**G**,**K**) Similarly, pharyngeal arch expression of *sox9a* is similar in wild-type and mutant embryos. (**H**,**I**,**L**,**M**) By 55 hpf, although the head is already noticeably smaller in mutants, patterning of *sox9a* is similar, highlighting the developing ethmoid plate, mandible, ceratohyal and ceratobranchials.